短　報

手術時視覚支援を目的とした赤外域スペクトル間演算の最適化

Optimization of Infrared Spectral Manipulation for Surgical Visual Aid

モンテイロ・シウドマール・タカハシ（学生会員）[a*],宇都有昭[a], 小杉幸夫[a], 小林信行[b], 渡辺英寿[b]
[a]東京工業大学メカノマイクロ工学専攻
[b]自治医科大学脳神経外科

Sildomar Takahashi Monteiro [a*], Kuniaki Uto [a], Yukio Kosugi [a], Nobuyuki Kobayashi [b], and Eiju Watanabe [b]
[a] Department of Mechano-Micro Engineering, Tokyo Institute of Technology
[b] Department of Surgical Neurology, Jichi Medical School Hospital

Abstract

During a surgical procedure, blood covering the surgical field hinders the surgeon's visual inspection. We propose a novel application of hyperspectral imagery in the biomedical field. We conceived a method to exploit the capabilities of hyperspectral imaging systems in order to provide clearer images of areas covered by blood to the surgeon. We developed a neural network approach to generate a nonlinear combination of spectral reflectance bands in the near infrared region revealing images that could not be seeing in unprocessed images. The experimental results are compared with conventional image processing techniques. We present *in vitro* experiments using human blood and *in situ* experiments using guinea pigs to attest the validity of the proposed method.

Key words

Image-guided surgery, Infrared medical imaging, Hyperspectral imagery, Neural networks, Spectral manipulation.

1．Introduction

Visual inspection is the most important guide to the microsurgery. Blood covering the surgical field is the largest obstacle to a proper surgical manipulation. The surgeon devotes a lot of time to keep the surgical field clean of blood. In addition, during especial procedures like minimally invasive surgery it is rather difficult to remove blood obstructing the surgeon's view. Successful surgery might come from bloodless operating field. If we could see through the blood layer, surgical time might decrease and the result would be better.

Imaging spectrometers have been developed to remotely measure and analyze the electromagnetic radiation of materials, at each wavelength and over a broad spectral band. By processing and combining spectral reflectance information from various non-visible wavelengths, we envision the possibility of revealing images under a superficial layer of blood

*東京工業大学大学院総合理工学研究科
〒226-8502 横浜市緑区長津田町 4259 番地 G2-16
monteiro@pms.titech.ac.jp
受付 2005 年 7 月 8 日； 採択 2006 年 6 月 2 日

that could not be seeing with the naked eye.

A previous work by W.-C. Lin, et al. [1] presents a different methodology aiming at reducing the effect of superficial blood contamination for *in vivo* tissue differentiation. They have employed the direct ratio of fluorescence and diffuse reflectance as the differential criteria for tissue discrimination. They demonstrated that this ratio, instead of solely the fluorescence spectrum, is less affected by superficial blood contamination for optical spectroscopy, in the range $\lambda = 300 \sim 600$nm. However, their method has a major limitation of relying on the assumption that the blood layer is extremely thin (less than 100 μm) and homogenous. This can only be satisfied using contact fiber-optic probes to acquire the data, and the validity of their assumption for non-contact spectral imaging modality (like ours) is not determined yet.

We developed a method using an artificial neural network (ANN) approach to provide a nonlinear combination of hyperspectral imagery data in order to produce a better visualization of the blood-covered area. Our method relies on the spectral reflectance in the near infrared region to generate an enhanced visualization of areas obstructed by a blood layer of up to 3mm of thickness.

2. Background

2. 1 Hyperspectral Imagery

Imaging spectrometers are able to sample the reflectance spectrum extending from the visible region ($\lambda = 400 \sim 700$nm) through the near infrared ($\lambda = 0.7 \sim 1.3\mu$m) to the mid infrared ($\lambda = 1.3 \sim 3.0\mu$m). The class of sensors capable of acquiring hundreds of narrow contiguous bands of information for spectral signature analysis is usually referred to as hyperspectral sensors [2]. In the field of remote sensing, many algorithms have been developed to extract scene information from spectral images, mainly aimed at pixels classification, material presence estimation, target detection and change detection [3].

In the biomedical field, optical spectrometers have been used for pathology sample analysis, live cell microscopy, non-invasive blood and other fluids analysis [4) 5)]. Fiber-optical reflectometers have been the main spectroscopy equipment utilized. Nevertheless, performing the spectral measurement in an imaging format has appealing advantages. For instance, the measurement can be done without physical contact, many points can be measured simultaneously, and it can be performed with minimal disturbance, i.e., without interfering with the surgeon's field of view.

2. 2 Blood Spectral Characteristics

The optical absorption properties of tissue in the ultraviolet, visible and near infrared regions are dominated by the absorptions of proteins, DNA, melanin, hemoglobin and water [6].

In the case of blood, hemoglobin and water are the basic components and main chromophores. While hemoglobin dominates the absorption properties in the visible spectrum, as we go to the near and mid infrared, water becomes the principal responsible for absorption. **Fig. 1** shows the optical absorption profile of hemoglobin and water in the spectrum. Note that the precise absorbance value of the blood-water solution at a given wavelength is inherently dependent on the layer thickness and on the hemoglobin concentration.

We considered that the determination of significant wavelengths and the optimum data combination to permit visualization under a layer of blood is a non-trivial problem that may require a nonlinear solution.

3. Methodology

3. 1 Image Processing Procedure

Fig. 2 shows the experimental data acquisition setup. It consists of light sources (a pair of 500W halogen lamps) a computer-controlled moving table,

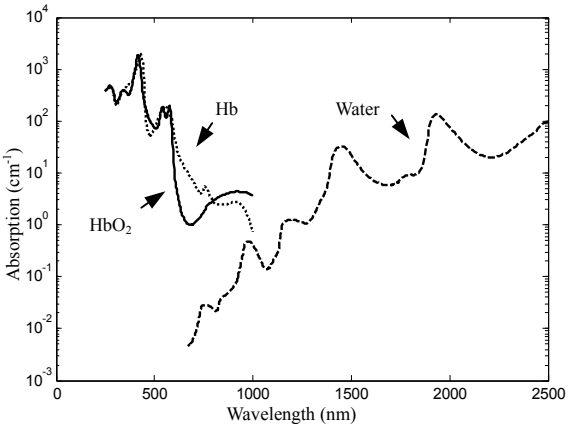

Fig. 1 Optical absorption curves of water and haemoglobin (Hb and HbO_2) in the range λ = 250~2500 nm; based on data gathered by Prahl [7].

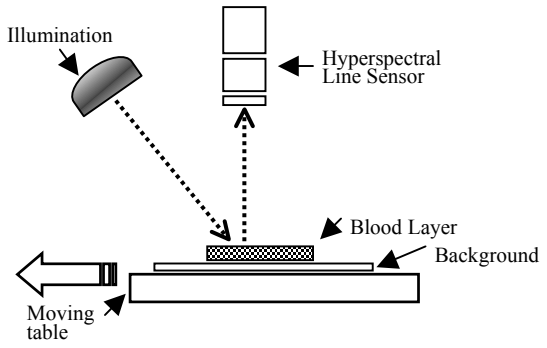

Fig. 2 Diagram of the experimental setup for the hyperspectral data acquisition.

and the hyperspectral line sensor.

In order to remove the spectral non-uniformity of the illumination device and influence of the dark current, we have normalized the radiance data to yield the radiance of the specimen. For this pre-processing, two auxiliary data were acquired during the experiments: the radiance of a standard reference white board placed in the scene, and the dark current measured by keeping the camera shutter closed. The raw data was then corrected to reflectance using the following equation:

$$R(\lambda) = \frac{I_{raw}(\lambda) - I_{dark}(\lambda)}{I_{white}(\lambda) - I_{dark}(\lambda)}, \tag{1}$$

where $R(\lambda)$ is the calculated reflectance value, for each wavelength; $I_{raw}(\lambda)$ is the raw data radiance value of a given pixel; and $I_{dark}(\lambda)$ and $I_{white}(\lambda)$ are, respectively, the dark current and the white board radiance acquired for each line and spectral band of the sensor.

3．2 Neural Network

ANNs provide a general and practical method for approximating complex nonlinear functions from examples [8]. ANNs have been successfully applied to a wide range of applications in remote sensing, medical data analysis and image processing [9].

We initially developed an image processing method using a single-layer perceptron (SLP) [11]. Each pixel value of the output image, can be expressed as

$$y = g\left(\sum_{m=1}^{M} w_m R(\lambda_m) + b\right), \tag{2}$$

where w_m represents the synaptic weights of the perceptron; $R(\lambda_m)$ is the reflectance of the specimen at $\lambda = \lambda_m (m = 1 \cdots M)$ to be applied to the perceptron; and b is the bias.

Another ANN architecture proposed was a multi-layer perceptron (MLP) feed-forward network trained by the back-propagation algorithm with momentum[12].

We codified the image using the discrete thermometer encoding, as described by T. O. Jackson [14], due to the difficulty presented by the neural network in providing a good output generalization when dealing with continuous data such as the pixel image information. The thermometer code can be expressed in the following manner:

$$\left.\begin{matrix} a_1 \\ a_2 \\ \vdots \\ a_k \end{matrix}\right\} = (+1) iff \begin{cases} x \geq u + \delta \\ x \geq u + 2\delta \\ \vdots \\ x \geq u + n\delta \end{cases}, \tag{3}$$

where n is the number of nodes; a_n is the output activation of unit n; and δ is the interval size given by $(v-u)/n+1$.

To obtain a two-level (black or white) representation of the image, we defined the number of nodes in the discrete thermometer scheme n = 1 to produce a binary output. For this case, only one neuron in the output layer is sufficient.

To generate a grey-scale representation, we defined the number of nodes as n = 128, thus producing 128 halftone levels. This encoding requires 128 nodes in the output layer to be represented.

Both ANN architectures need 150 input nodes, which is the number of effective spectral channels of the hyperspectral sensor utilized. The number of nodes in the hidden layer of the MLP was determined experimentally as 10.

The hyperspectral data is processed by the ANNs as follows. First, we manually select the image region to be used for training (input and target) and testing. Tutorial images without blood are used as target, and the same scene covered by blood are the inputs. Second, the reflectance value is normalized and converted to fall in the range [-1, 1]. Thirdly, the target data is coded using the discrete thermometer scheme. Fourthly, the ANN is trained until the mean squared error falls to zero or the maximum epoch is

reached. Finally, the output generated by the ANN is decoded from the discrete thermometer scheme to a desired image format, e.g., binary or 8 bits grey-scale.

4. Experiments

We utilized a hyperspectral imaging spectrograph ImSpector N17(E), which produces 160 wavelength channels interleaved by 5 nm of distance in the range $\lambda = 900 \sim 1700\text{nm}$ [15]. The CCD sensor scans the scene in two dimensions, one in the space (image line information) and, the other, in the electromagnetic spectrum (spectral information).

4. 1 *In vitro* Experiment using Human Blood

For our preliminary experiments, we analyzed the spectral data of a solution of hepaline-added human blood (70%) and saline water (30%), with approximately 3 mm of thickness, poured in an uncovered Petri dish [10]. As background scene, we utilized a calendar print with black characters, as shown in **Fig. 3**.

A sample area, around the calendar's number five submerged in the blood, was processed. In order to compare the results, we manually picked the single band presenting the clearest visualization of the blood-affected area, λ = 1260 nm. Then, we processed the image with the conventional technique of binary conversion using a threshold. The results of the conventional image processing method, SLP, and MLP, for the binary output case, are shown in **Fig. 4**. For all cases, the training set consisted of the image area in the upper part of the number five without blood, as highlighted by the rectangle in **Fig. 5(a)**.

Next, we processed the picked image with the traditional technique of contrast stretching. The results of the conventional image processing method and the MLP, for the grey-scale image, are presented in **Fig. 5(b)** and **Fig. 5(c)**.

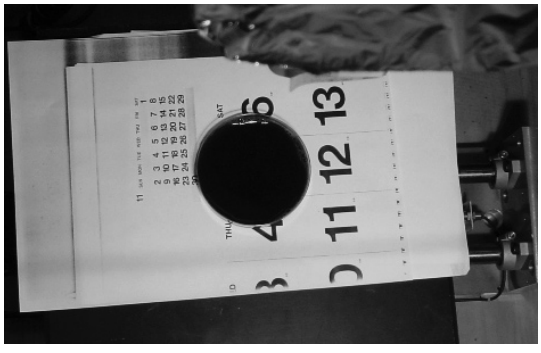

Fig. 3 *In vitro* experimental setup; Petri dish with human blood on top of a calendar as background.

(a) (b) (c)

Fig. 4 Human blood experiment results: comparison of binary images of a sample area after processing: (a) binary conversion using a threshold, image of λ = 1260 nm; (b) single-layer perceptron output; (c) multi-layer perceptron output.

(a) (b) (c)

Fig. 5 Comparison of grey-scale images: (a) Tutorial image without blood; (a) contrast stretched image of λ = 1260 nm; (b) multi-layer perceptron output.

4. 2 *In situ* Experiment using Guinea Pig

The following experiments were performed using a guinea pig and its blood. The blood was diluted in saline water with nearly 50% of proportion. A specific acrylic box was designed in order to guarantee a uniform thickness of the blood layer. The box has 0.3mm thick top and bottom lids, which provides a transparency of approximately 95%, and walls with uniform height of 3 mm. We present the results of the experiment using the guinea pig abdomen as background; the experimental setup is shown in **Fig. 6**.

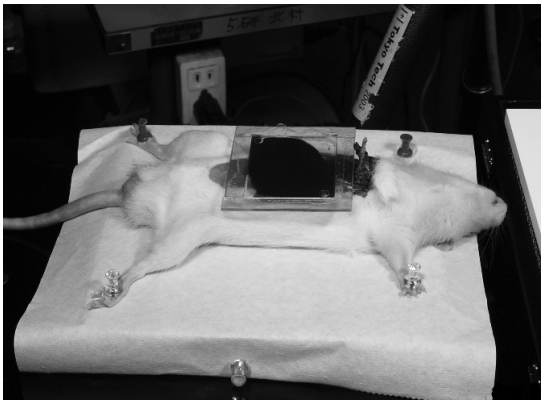

Fig. 6 *In situ* experimental setup; acrylic box filled with blood on top of guinea pig's opened abdomen.

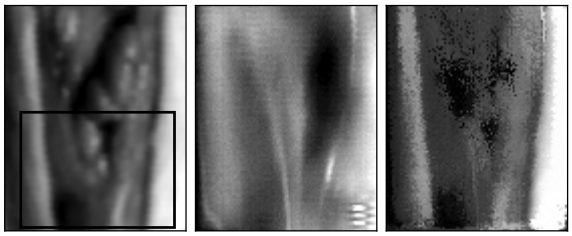

(a) (b) (c)

Fig. 7 Guinea pig experiment results: comparison of grey-scale images: (a) Tutorial image without blood; (b) Contrast stretched image of λ = 1100nm; (c) Multi layer perceptron output.

The training set consisted of the image area in the lower part of the abdominal area without blood, highlighted by the rectangle in **Fig. 7(a)**. As in the *in vitro* case, a comparison with a conventional image processing technique is presented in **Fig. 7(b)**. Finally, the output of the neural network is presented in **Fig. 7(c)**.

4．3 ANN Learning Analysis

To follow the effective learning of the ANN, we produced binary images processed by the MLP at several early epochs of the learning process. A montage with the resulting images is shown in **Fig. 8**. The stopping criterion to generate the images was 20% decay from the mean squared error value of the previous image. As weights are set randomly in the beginning, early images generated by the ANN are very noisy, but as the learning steps advance, output images become more and more definite. The final image was obtained after the training algorithm had stopped completely.

The long-term knowledge of an ANN is stored in the strength of the weighted connections between units. The characteristics of the SLP allow the verification of its weight vector, w_m in equation (2), which is presented in a graphical format in **Fig. 9**. This provides an empirical insight of how the wavelengths are automatically weighed by the learning algorithm. The figures show that spectral channels in the interval from λ = 1000 *n*m to λ = 1300 *n*m have received higher weight values by the SLP, thus presenting more significance on the composition of the visualization output.

4．4 Discussion

The contrast stretching method and threshold binary transformation presented the less distinctive

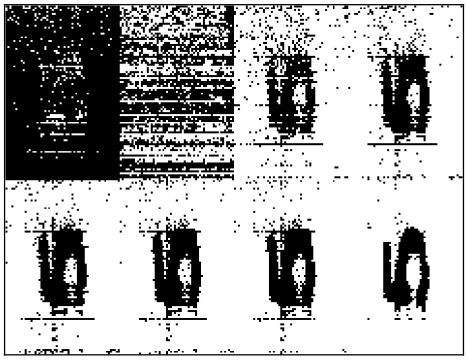

Fig. 8 Composite picture of sample images generated during the training process of the multi-layer perceptron. Training epochs are, from top left, respectively: 1, 67, 138, 214, 294, 383, 563 and 2000.

images. The SLP was able to learn an improved visualization. The MLP generated the clearest visualization of the background covered with blood. The main advantage of ANN is its ability to learn from example and generalize this result to other samples, which have not been presented to the ANN yet. Conventional image processing methods usually require an elaborate examination of the hyperspectral data to generate a single image. Nevertheless, ANN presents the difficulty of architecture design, typically a trial and error procedure, and has an intrinsic sensibility to the quality and diversity of the training data set.

To extract significant information under a layer of stained blood two constraints must be respected, that the light source is sufficiently powerful and the layer is thin (up to 3mm in our observations). Nevertheless, if the layer of blood and the region of interest are not in physical contact, due to optical limitations, it becomes difficult to obtain significant information, even in the wavelengths of blood's less optical absorption. This factor may have affected the quality of the data acquired in the guinea pig's experiment, where a small space between the bottom of the acrylic box and the Guinea pig's organs was observed.

The hyperspectral line sensor that we have been using may represent a shortcoming for our method. Since it is necessary to line-scan the image, its practical use is limited. A visual aid tool to be used during surgical procedures demands a faster imaging method. To circumvent the problem, one possible approach is to limit the number of spectral-channel inputs in the ANN in order to allow the acquisition of multi-spectral bands in two spatial dimensions (im-

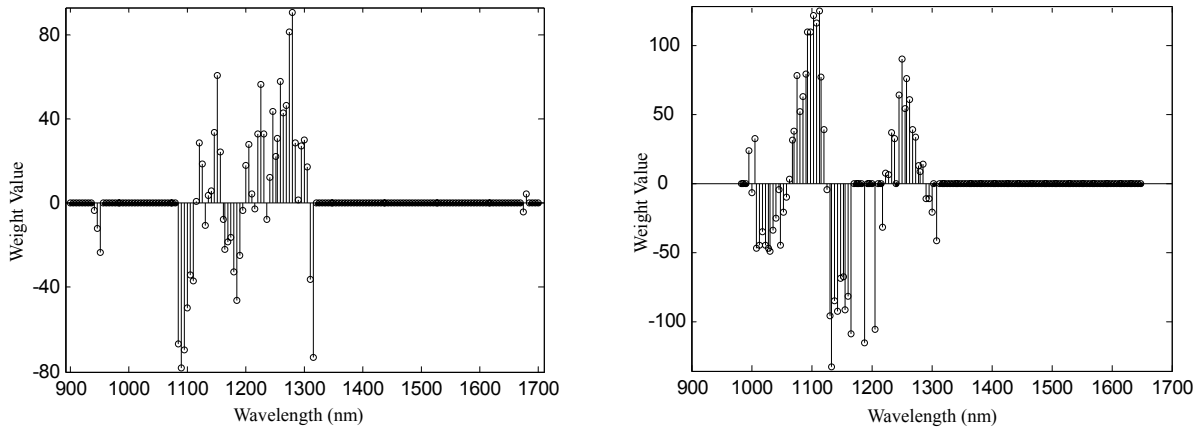

Fig. 9 Final weights configuration of the SLP, referred to each spectral channel of the hyperspectral sensor: a) case of *in vitro* experiment using human blood; b) case of *in situ* experiment using guinea pig.

ages, not lines) at real time.

The usefulness the SLP is that the connecting weights can be interpreted as the significance of the spectral components of the input. Moreover, by approximating the weight series with an optical filter bank, we were able to design a multi-spectral camera for real-time 2-D image acquisition, without requiring the scanning mechanism [13].

5. Conclusion

The main contribution of this paper is to propose a novel biomedical application for hyperspectral imaging systems. The results reported indicate the possibility of exploiting a region of low optical absorption presented by the blood in order to generate an enhanced image of a submerged region. The proposed ANN-based method proved able to learn how to combine the reflectance data from various spectral bands and generate a visualization of the area obstructed under the layer of blood.

The straightforward application of the proposed method is in the biomedical field, for surgical guidance. Other application would be to improve the method to look at skin and tissue surface through bloody gauze or bandage without the need to remove them, facilitating the diagnosis. Extensions of the technique to other substances could also be developed and applied to diverse fields such as arts (work of art analysis) and agriculture (remote crop assessment).

References

1) Lin W-C, Toms SA, Jansen ED, Mahadevan-Jansen A. Intraoperative application of optical spectroscopy in the presence of blood. IEEE Journal of Selected Topics in Quantum Electronics 2001; 7(6):996-1003.
2) Richards JA, Jia X. Remote Sensing Digital Image Analysis, An Introduction. 3rd Edition. New York: Springer-Verlag, 1999.
3) Mather PM. Computer Processing of Remotely-Sensed Images, An Introduction. Chichester: John Wiley & Sons, 2004.
4) Levenson RM. Spectral Imaging and Pathology: Seeing More. Laboratory Medicine 2004; 35(4): 244-251.
5) Zimmermann T, Rietdorf J, Pepperkok R. Spectral imaging and its applications in live cell microscopy. FEBS Letters 2003; 546(1):87-92.
6) Vogel A, Venugopalan V. Mechanisms of pulsed laser ablation of biological tissues. Chemical Reviews 2003; 103(2): 577-644,.
7) Prahl S. Optical Properties Spectra of Hemoglobin and Water. Oregon Medical Laser Center, 2001. Online available: http://omlc.ogi.edu/spectra/
8) Mitchell TM. Machine Learning. Boston: McGraw-Hill, 1997.
9) Egmont-Petersen M, Ridder D, Handels H. Image Processing with neural networks – a review. Pattern Recognition 2002; 35: 2279-2301.
10) Monteiro ST, Kosugi Y, Uto K, Watanabe E. Towards Applying hyperspectral Imagery as an Intraoperative Visual Aid Tool. Proceedings of the fourth International Conference on Visualization, Imaging and Image Processing, Marbella, 2004: 483-488.
11) Bishop CM. Neural networks for pattern recognition. New York: Oxford University Press, 1995.
12) Haykin S. Neural Networks: A Comprehensive Foundation. 2nd ed. Englewood Cliffs: Prentice-Hall, 1999.
13) Monteiro ST, Uto K, Kosugi Y, Watanabe E. Towards a Surgical Tool Using Hyperspectral Imagery as Visual Aid. Proceedings of the International Workshop on Augmented Environments for Medical Imaging and Computer-aided Surgery 2004, in conjunction with MICCAI. Rennes, 2004: 97-103.
14) Jackson TO. Data Preprocessing. In: Fiesler E, Beale R, eds. Handbook of Neural Computation. New York: Institute of Physics and Oxford University Press, 1997.
15) Spectral Imaging Ltd. ImSpector Imaging Spectrograph User Manual. Version 2.21. Oulu 2003.